Supporting information

Dipole-Assisted Nanoporous Networks on Surfaces

Huanjing Luo,[†▽] Andrea Minoia,[‡] Vipin Mishra,[†▽] Dariane Fadoras,[‡] Filippo Giovanni Fabozzi,[#] Roberto Lazzaroni,[‡] Stefan Hecht,[#] Kunal S. Mali,[†▽]* and Steven De Feyter[†▽]*

[†]Division of Molecular Imaging and Photonics, Department of Chemistry, KU Leuven, Celestijnenlaan 200F, 3001 Leuven, Belgium; [▽]KU Leuven Institute for Micro- and Nanoscale Integration (LIMNI), Celestijnenlaan 200F, KU Leuven, 3001 Leuven, Belgium; *[‡]Laboratory for Chemistry of Novel Materials, University of Mons, Place du Parc 20, 7000 Mons, Belgium; [#]Department of Chemistry and Center for the Science of Materials, Berlin, Humboldt-Universität zu Berlin, 12489 Berlin, Germany*

Corresponding authors:

Kunal S. Mali (kunal.mali@kuleuven.be)

Steven De Feyter (steven.defeyter@kuleuven.be)

Table of Contents:

Section 1. Synthesis of 1 and 2

Commercially available chemicals and solvents were bought *via* Sigma Aldrich, TCI Chemicals, Acros Organics, and Apollo Scientific, and used without further purification. Column chromatography purifications were performed using a Biotage Isolera One Flash Purification Chromatography. For UPLC-MS, a Waters UPLC Acquity with a Waters Alliance System (Waters Separations Module 2695, Waters Diode Array Detector 996, and Waters Mass Detector ZQ 2000) was used. HR-MS measurements were performed on a Xevo G3 QTof. Nuclear magnetic resonance (NMR) spectra were recorded using a Bruker AV III HD Spectrometer (600 MHz for 1H).

2,4,6-Tris[4-(cyanomethyl)phenyl]-1,3,5-triazine (**1**) was synthesized and characterized following a reported[1] procedure. 1,3,5-Tris(4-cyanomethylphenyl)benzene (**2**) was synthesized following a modified literature procedure.[2] 1,3,5-tribromobenzene (200 mg, 0.635 mmol), 4-(methylcyano)phenyl boronic acid (0.767 mg, 4.76 mmol), K_2CO_3 (708 mg, 8.07 mmol), and $Pd(PPh_3)_4$ (70.8 mg, 0.061 mmol) were added to a round-bottom flask, and after evacuation, N_2 was back refilled three times. Dioxane (133 mL) and water (27 mL) were then added, and the resulting suspension was degassed with N_2 for 30 min. The reaction mixture was subsequently heated at 100 °C and stirred for 3 days. After completion as judged by TLC, the mixture was extracted with DCM and washed with water and brine, dried with $MgSO_4$, and the solvent removed under reduced pressure. The resulting crude solid residue was purified by flash column chromatography (SiO_2, cyclohexane: ethyl acetate = 1:1). The final product **2** was obtained as a pale yellow solid (247 mg, 0.582 mmol, 92%).

^{1}H NMR (400 MHz, DMSO-d_6): δ [ppm] = 7.75 (s, 3H), 7.70 (d, 6H), 7.46 (d, J = 8.0 Hz, 6H), 3.83 (s, 6H).

^{13}C NMR (75 MHz, DMSO-d_6): δ [ppm] = 141.02, 139.31, 130.86, 128.69, 127.80, 119.27, 22.08.

ESI+ MS *m/z* calculated for $C_{27}H_{18}N_6$: 424.1808, found: 424.1804.

Section 2. STM characterization

*2a. SAMN of **1**:* A stock solution was prepared by dissolving 0.17 mg of **1** in 1 mL of dimethyl sulfoxide (DMSO, >99.0 %, TCI Chemicals). This solution was then diluted 33-fold with ethanol to obtain a final concentration of 12 μM (containing 3 vol% DMSO). Approximately 5 μL of the diluted solution was drop-cast onto freshly cleaved highly oriented pyrolytic graphite (HOPG, grade ZYB, Advanced Ceramics Inc., Cleveland, USA). The substrate was sealed in a closed vessel and maintained under ambient conditions (21–23 °C) for two days. Afterwards, a drop of octanoic acid (OA, ≥99.5 %, Carl ROTH) was added to the sample, which was then characterized by STM at the HOPG/OA interface.

*2b. SAMN of **2**:* A stock solution was prepared by dissolving 0.56 mg of **2** in 1 mL of DMSO. This solution was then diluted 33-fold with ethanol to obtain a final concentration of 40 μM (containing 3 vol% DMSO). Approximately 5 μL of the diluted solution was drop-cast onto freshly cleaved HOPG. The

substrate was then sealed in a closed vessel and heated up at 80 °C for 1 hour. After cooling to room temperature, the sample was characterized by STM.

*2b. Host-guest SAMN of **1** and coronene:* The host SAMN was prepared as described in 2a (see above). After imaging the porous networks using STM, a drop of saturated coronene (COR) solution in heptanoic acid (HA) was drop-cast onto the surface. Coronene serves as the guest species. Once the COR solution had uniformly spread, the sample was recharacterized by STM.

2c. STM experiments: All STM experiments were performed at room temperature (21–23 °C) using a PicoSPM (Keysight Technologies) machine operating in constant-current mode with the tip immersed in the supernatant liquid. STM tips were prepared by mechanically cutting a Pt/Ir wire (80%/20%, diameter 0.2 mm). The experiments were repeated in 2-3 sessions using different tips to check for reproducibility and to avoid experimental artefacts, if any. For analysis purposes, recording of a monolayer image was followed by imaging the graphite substrate under the same experimental conditions, except for increasing the current and lowering the bias. The images were corrected for drift via Scanning Probe Image Processor (SPIP) software (Image Metrology ApS), using the recorded graphite images for calibration purposes, allowing a more accurate unit cell determination. The unit cell parameters were determined by examining at least four images, and only the average values are reported. The images are Gaussian filtered unless mentioned otherwise. The imaging parameters are indicated in the figure caption: tunneling current (I_{set}) and sample bias (V_{bias}).

Section 3. Computational methods

For this study, due to the possible complexity and size of the models, we rely on a force field-based modeling strategy. Modeling was conducted with the Biovia Materials Studio 2022 molecular modeling suite, and both DREIDING and PCFF force fields were tested with the aim of finding which one best reproduces the molecular geometry of the molecules in the gas phase. By comparing the chemical structure of molecules **1** and **2**, in fact, the nature of the core is expected to change the overall geometry of the molecule, with the phenyl core of molecule **2** promoting a twist of the three "arms", while a flatter geometry is expected for molecule **1**. Both force fields are predicting a flat geometry for molecule 1, but a different twist for molecule 2. To pick the best force field, we compare the twist these force fields predict for the biphenyl molecule in the gas phase with data from the literature.[3] We found the PCFF force field with ESP atomic charges derived from B3LYP/6-31g** DFT calculations well reproduces the position of the minima (~34°) and the height of the rotational barriers for the rotational energy profile of bithiophene. As per the orientation of the -CN groups, DFT calculations show that the rotational energy profile of the -CN group with respect to the phenyl ring is attached to is rather flat, while PCFF+ESP predicts a minimum when the -CN group and the phenyl ring are coplanar, as expected to be once the molecule is adsorbed on the HOPG graphite surface. For these reasons, all force field simulations were conducted with the PCFF force field using DFT ESP atomic charges.

Section 4. Supporting data

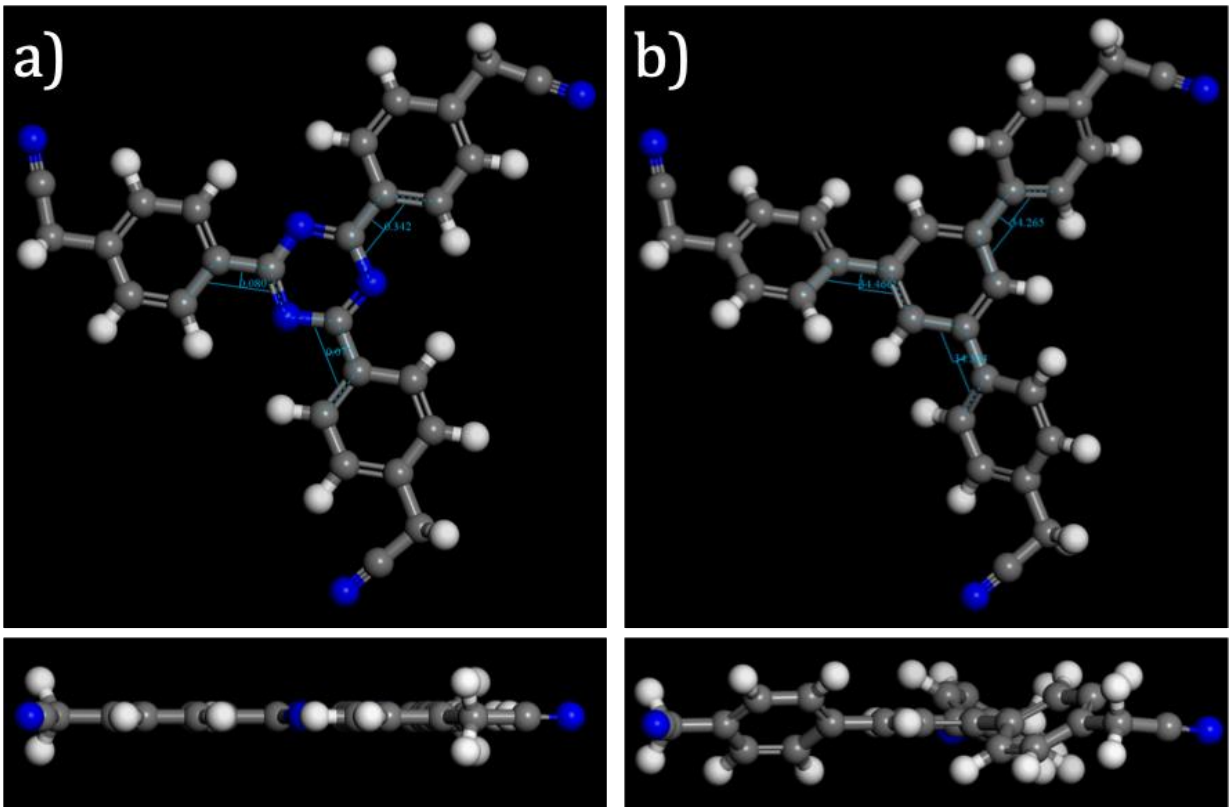

Figure S1. Molecular conformation of **1** (a) and **2** (b) in the gas phase obtained using the PCFF force field. The model shows that **1** exhibits a planar conformation, whereas **2** is non-planar with the phenyl arms tilted at 34° with respect to the central phenyl core (see bottom panels for the side views).

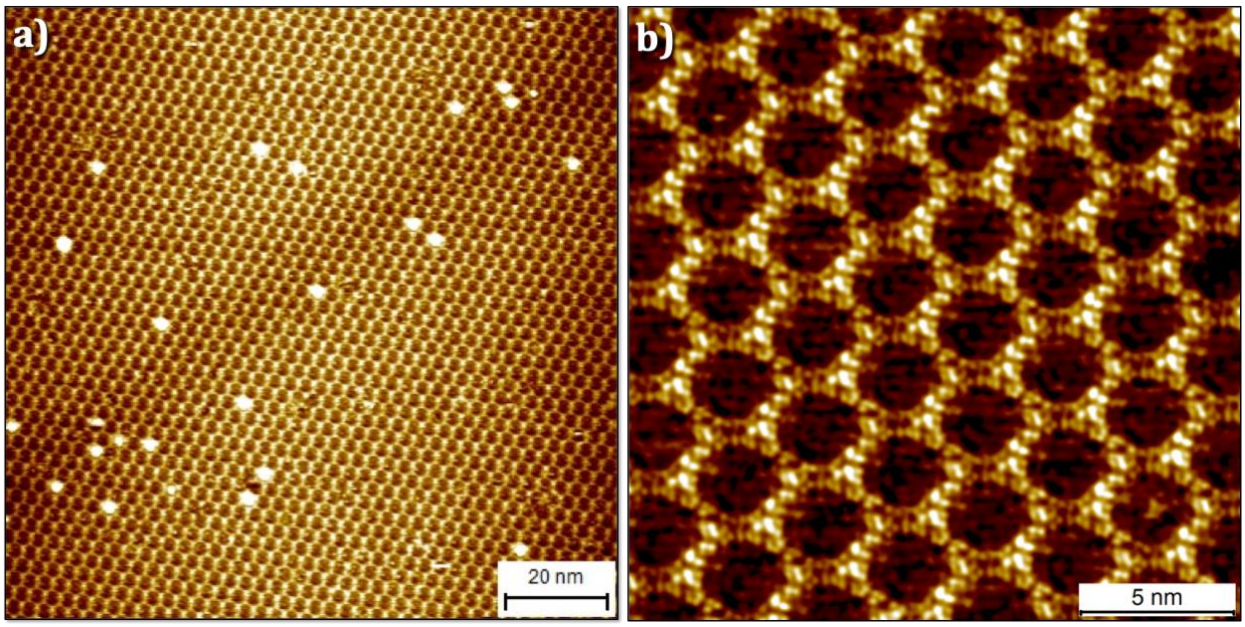

Figure S2. Large (a) and small-scale STM images of SAMN of **1** imaged at the OA/HOPG interface. Imaging parameters: (a) I_{set} = 100 pA, V_{bias} = –1000 mV (b) I_{set} = 100 pA, V_{bias} = –900 mV.

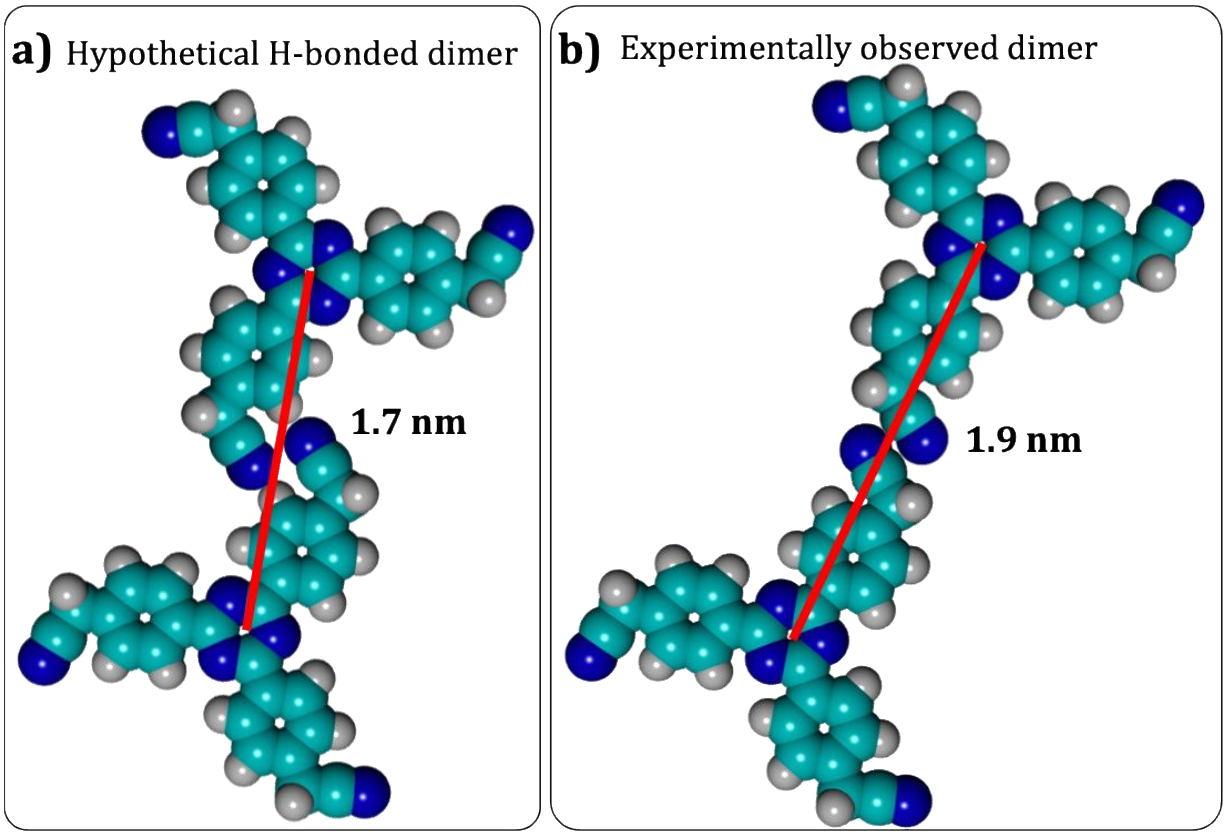

Figure S3. A comparison of the hypothetical H-bonded dimer of **1** *versus* the experimentally observed dipole-directed dimer of **1**.

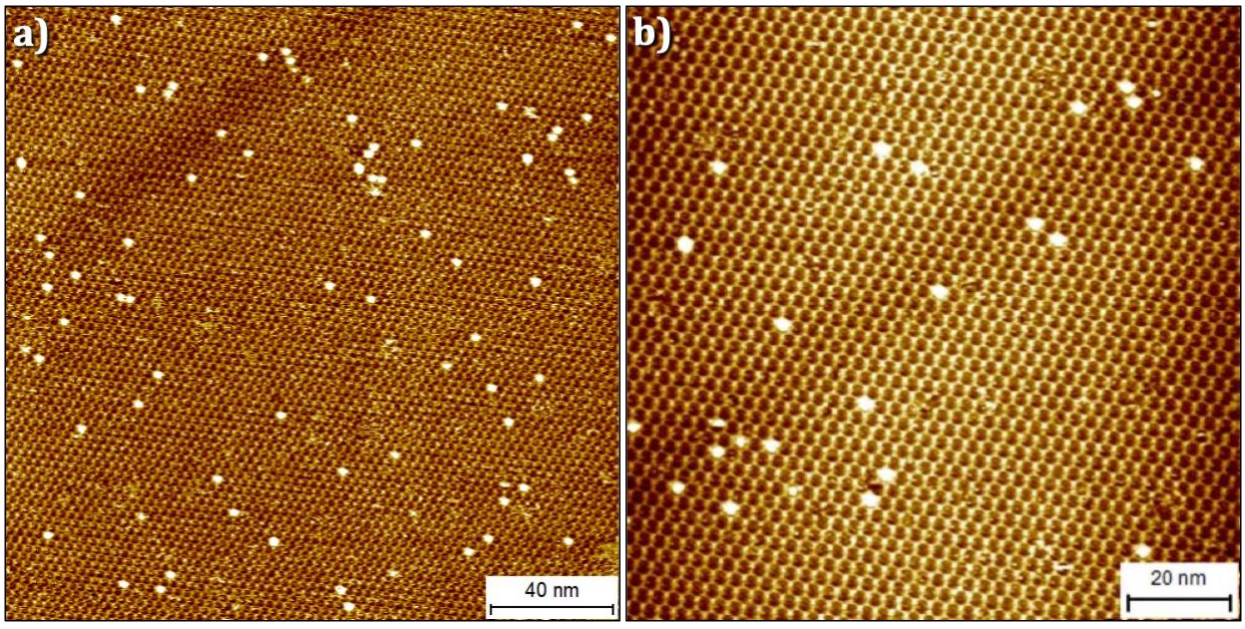

Figure S4. Large-scale STM images showing improvement in the crystallinity and domain sizes upon annealing of the SAMNs of **1** formed on the graphite substrate. Imaging parameters: (a) I_{set} = 100 pA, V_{bias} = -1000 mV (b) I_{set} = 100 pA, V_{bias} = -1000 mV.

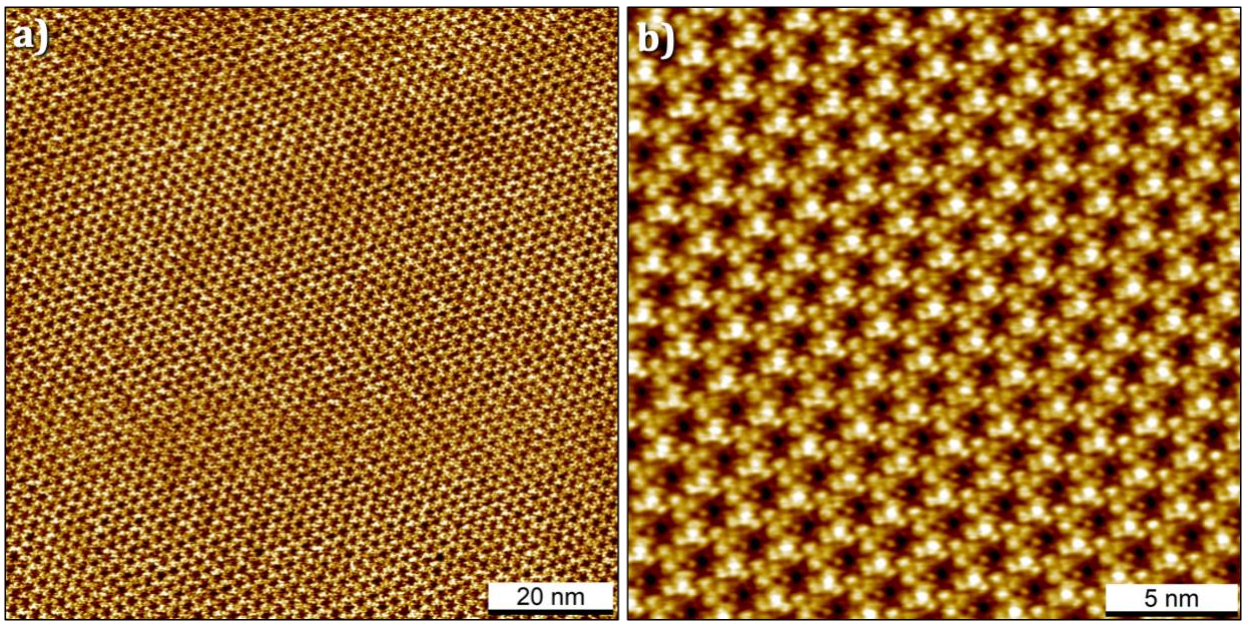

Figure S5. Large (a) and small (b) STM images of SAMN of **2** imaged at the OA/HOPG interface. Imaging parameters: (a) I_{set} = 100 pA, V_{bias} = -1000 mV (b) I_{set} = 100 pA, V_{bias} = –1000 mV.

Section 5. MM optimized models of molecular dimers

To rationalize the different SAMNs formed by molecules **1** and **2**, we systematically investigated the stability of the various dimer configurations that can be formed on the surface. At this stage, solvent effects are not considered and will be discussed later. Figure S6 presents a schematic representation of the dimers considered, which differ in the relative position of the molecules and in the orientation of their -CN groups. Among the possible configurations, the head-to-head (HH) and the side-by-side (SS1, SS2, SS3) dimers are the most relevant. Notably, the SS1 and SS2 dimers differ in the way the -CN groups are oriented when interacting with the core of the adjacent molecule.

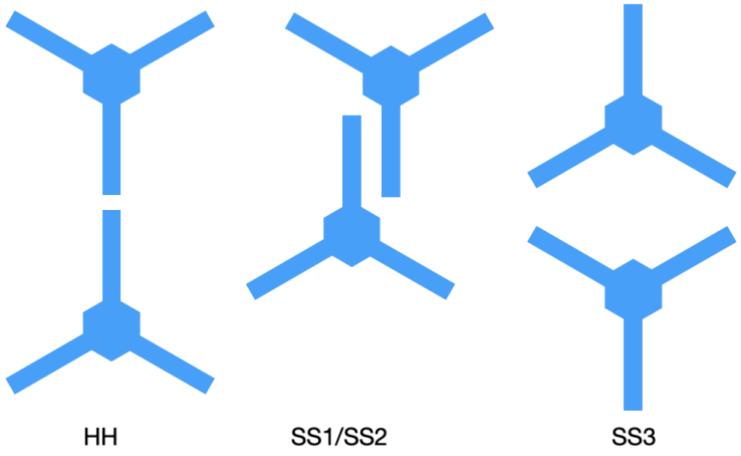

Figure S6. A schematic representation of the dimer molecules **1** and **2** could form on the surface.

Figures S7 to S10 compare the optimized structures of these dimers formed by molecules **1** and **2**.

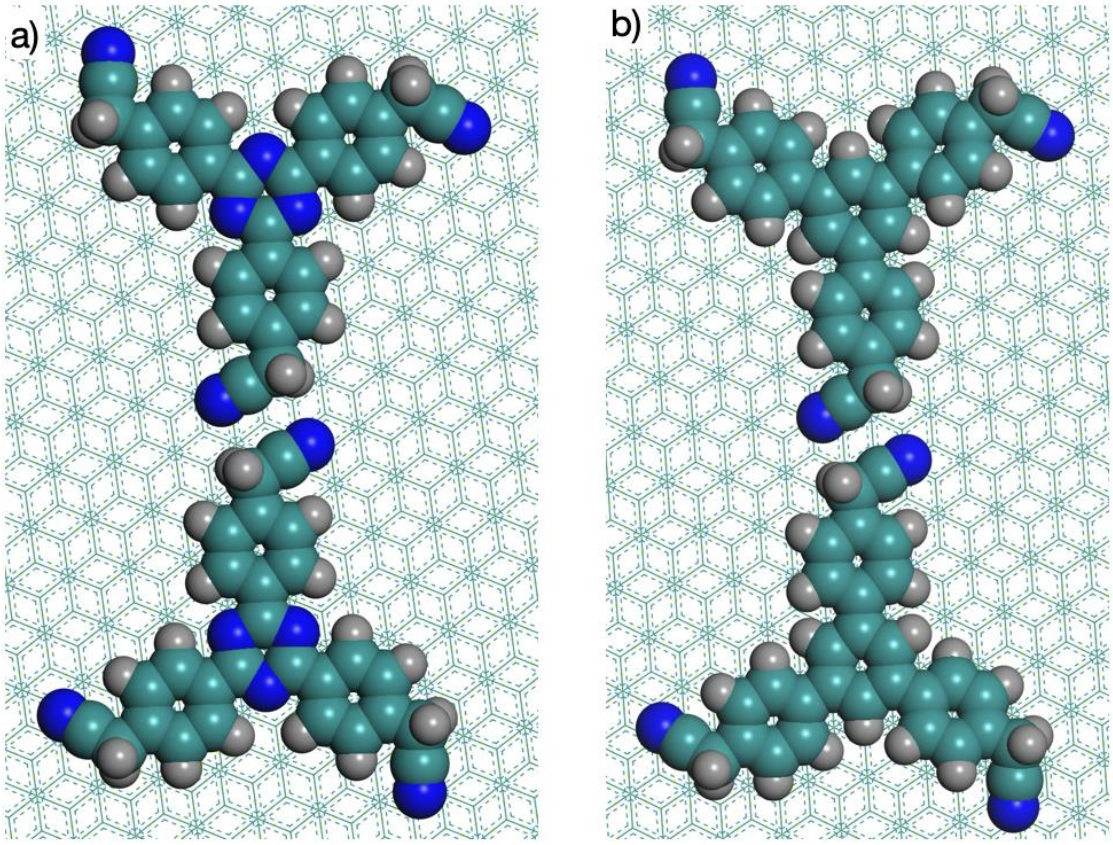

Figure S7. Head-to-Head (HH), dimers formed by (a) molecule **1** (E_{Int} = -4.6 kcal/mol) and (b) molecule **2** (E_{Int} = -4.7 kcal/mol).

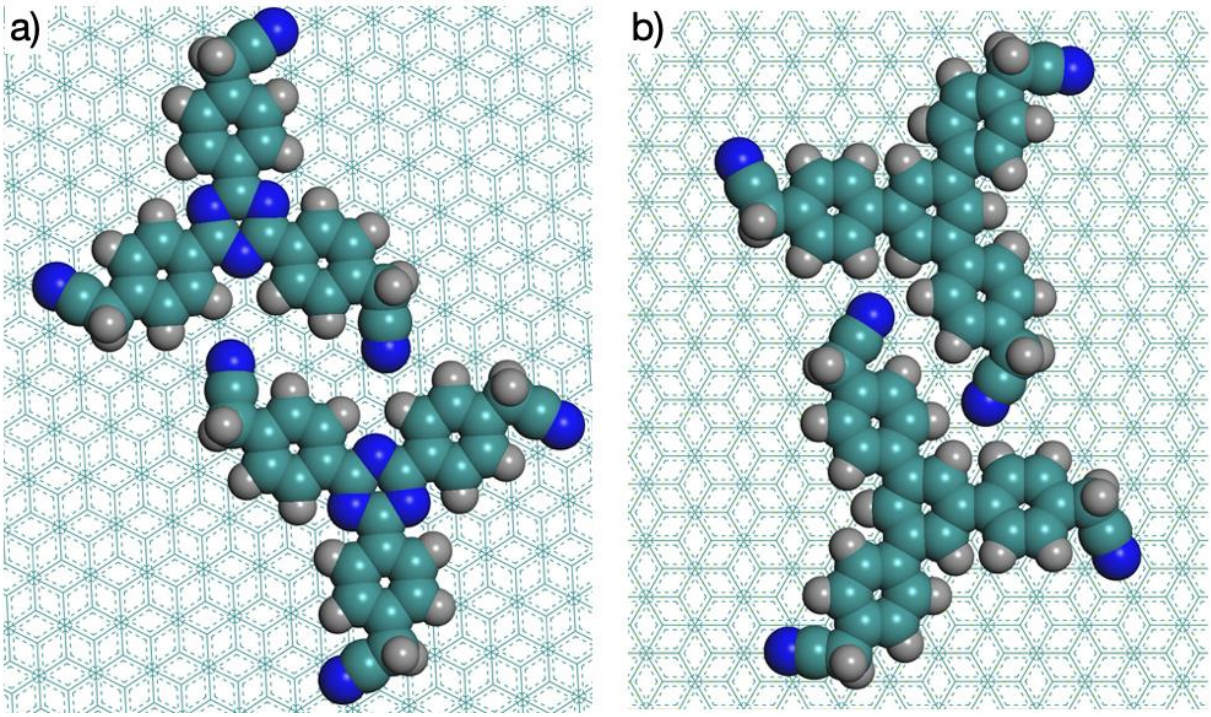

Figure S8. Side-by-Side (SS1) dimers formed by (a) molecule **1** (E_{Int} = -4.7 kcal/mol) and (b) molecule **2** (E_{Int} = -7.6 kcal/mol).

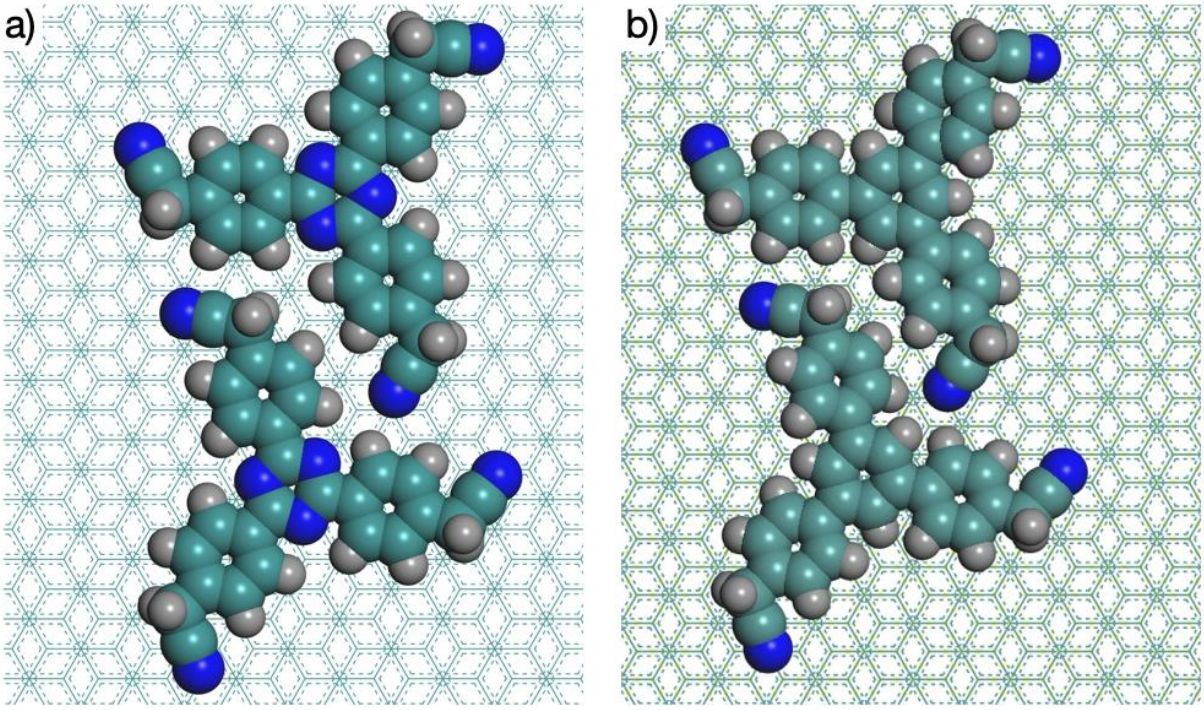

Figure S9. Side-by-Side (SS2) dimers formed by a pair of (a) molecule **1** (E_{Int} = -4.7 kcal/mol) and (b) molecule **2** (E_{Int} = -7.6 kcal/mol).

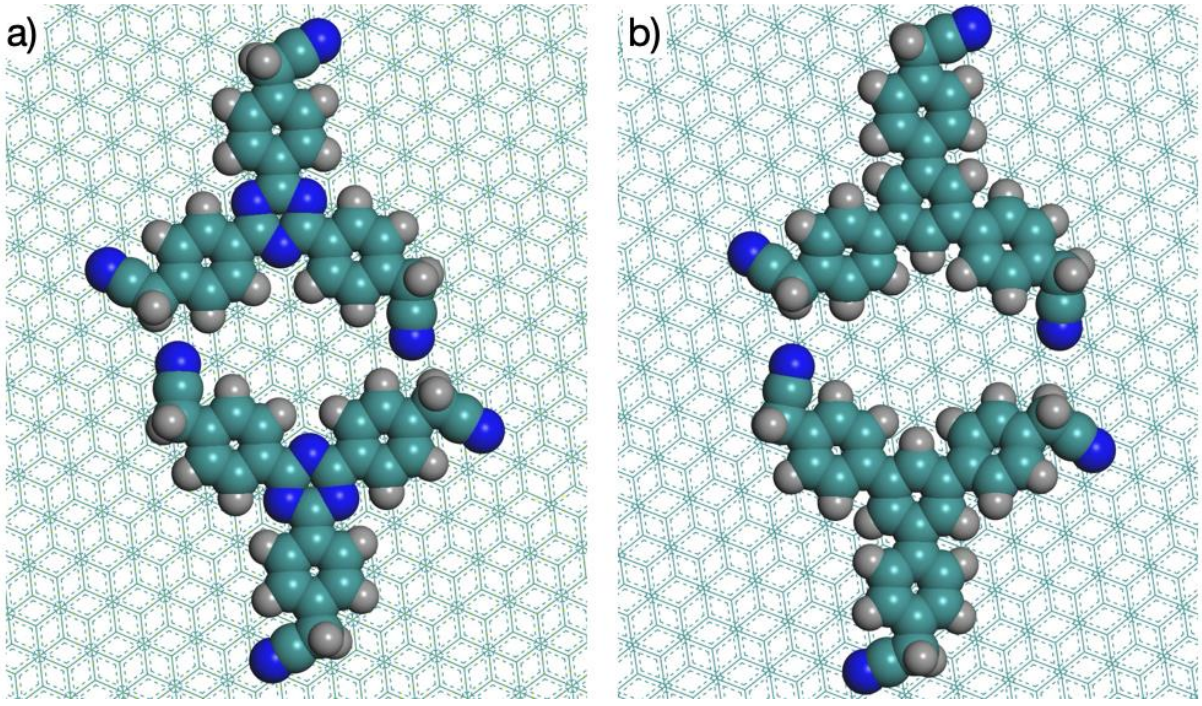

Figure S10. Side-by-Side (SS3) dimers formed by a pair of (a) molecule **1** (E_{Int} = -7.2 kcal/mol) and (b) molecule **2** (E_{Int} = -8.6 kcal/mol).

The intermolecular interaction energy, E_{int}, for all the investigated dimers are reported in Table SM1.

Table S1. Interaction energy, E_{INT}, for all dimers of molecules **1** and **2**.

	HH	**SS1**	**SS2**	**SS3**
Mol **1** E_{int} (kcal/mol)	-4.6	-4.7	-4.7	-7.2
Mol **2** E_{int} (kcal/mol	-4.7	-7.6	-7.6	-8.6

For molecule **1**, the underlying populations of dimers at the surface are composed of three dimer types, *i.e.,* HH, SS1, and SS2, for which the molecules have very similar interaction energy, while SS3 dimers are the ones with the strongest intermolecular interactions. This picture is different for molecule **2**. Here, the molecules strongly interact when forming the SS1, SS2, and SS3 dimers, while their interaction is the weakest for the HH dimer. This analysis suggests that the type of dipole-dipole interactions that are present in the HH dimers is not strong enough to stabilize the dimer, and the relative strength of the intermolecular interactions within dimers of **1** and **2** does not explain the formation of the two different monolayers experimentally observed.

Section 6. The role of the solvent in SAMN formation

Since the molecular models were initially built under "dry" conditions, *i.e.,* without considering solvent effects, they could not explain the experimentally observed formation of monolayers. To address this, additional molecular models were built, which included the solvent molecules to estimate the strength of solvent–molecule interactions and to clarify the role of the solvent in promoting monolayer formation. In particular, heptanoic acid is expected to form hydrogen bonds with the nitrogen atoms of the nitrile group. Since PCFF lacks a dedicated energy term for hydrogen bonding, the energies of the PCFF-derived structures were re-evaluated using the DREIDING force field, which explicitly accounts for H-bonding interactions. The energy of a single H-bond formed between a solvent molecule and the -CN groups **(Figure S11)** is calculated to be –3.7 kcal/mol.

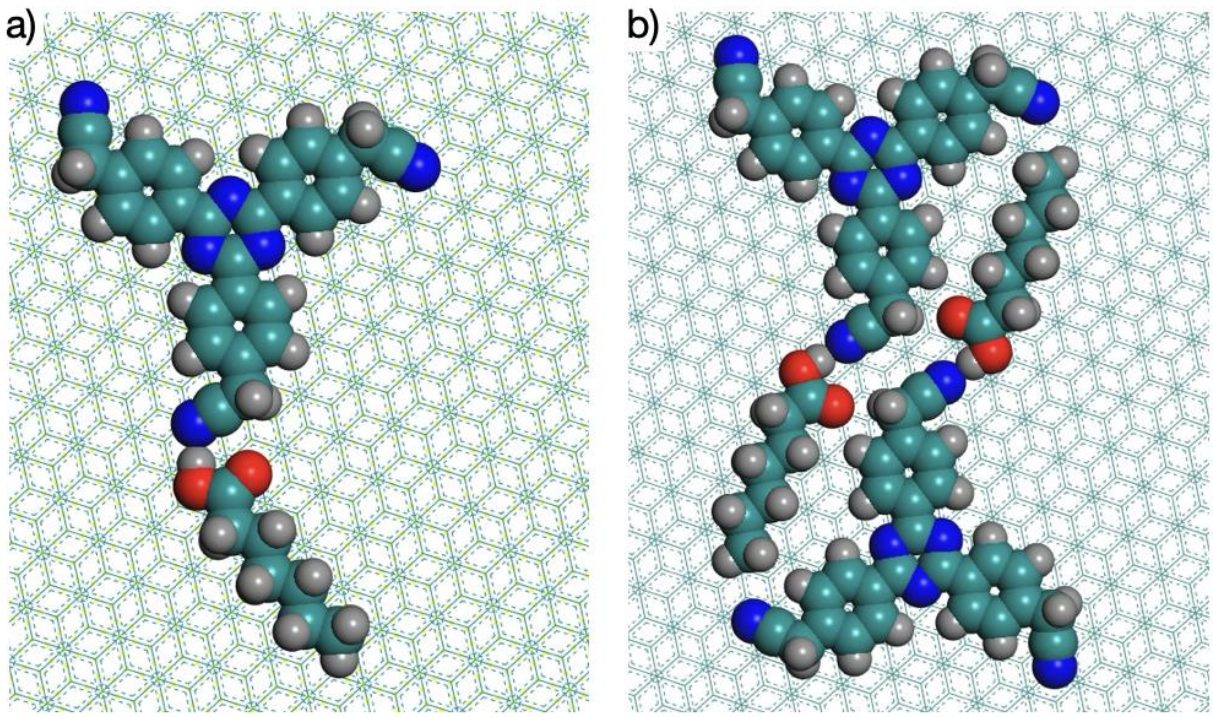

Figure S11. (a) Molecular model showing the favorable hydrogen bonding interaction between molecule **1** and the solvent. (b) Optimized structure for a solvent-stabilized HH dimer of molecule **1**.

Two solvent molecules, Figure **S11**, can stabilize a HH dimer, thanks to the favorable vdW interactions and the formation of the H-bonds.

This stabilization occurs for HH dimers of both molecules **1** and molecules **2**: once again, by considering the stability of geometry geometry-optimized solvated dimer does not offer a clear clue to explain the experimental results. 200 ps-long MD simulations on the solvated HH dimers of **1** and **2** were conducted in the NVT ensemble at 300K to capture the dynamic behavior of the dimers in the presence of solvent molecules. The analysis of the MD trajectories reveals that both HH dimers are quite dynamic despite the presence of the solvent, and that while dimers from molecules **1** can stay mostly in a HH conformation, those formed by molecules **2** will mostly get trapped in SS1/SS2 orientations. This is mostly due to the strong intermolecular interaction within the SS dimers of molecule **2**: despite the solvent, once an HH dimer switches to a SS conformation during the MD, it never goes back to being HH. The dynamic behavior of the dimers of molecule **2** strongly suggests that these will mostly aggregate in SS dimers, leading to the more compact assembly observed experimentally. On the other hand, for molecule 1, HH and SS dimers can more easily interconvert, with the HH ones more efficiently stabilized by the interactions with the solvent molecules on the surface. This suggests that molecules 1 tend to aggregate in HH dimers, *i.e.,* the precursors of the observed nanoporous network.

A monolayer (Figure S12) built with the dimers shown in Figure S11b has a unit cell (a, b, γ) = (3.3nm, 3.2nm, 58º) that matches the experimental one (a, b, γ) = (3.1±0.2nm, 3.1±0.2nm, 60±4º).

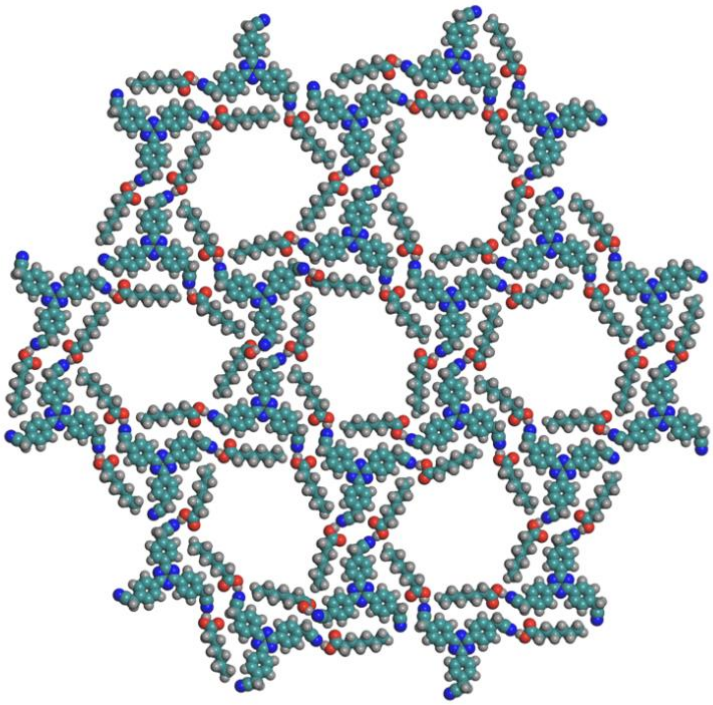

Figure S12. Nanoporous SAMN of molecule **1**, stabilized by the solvent.

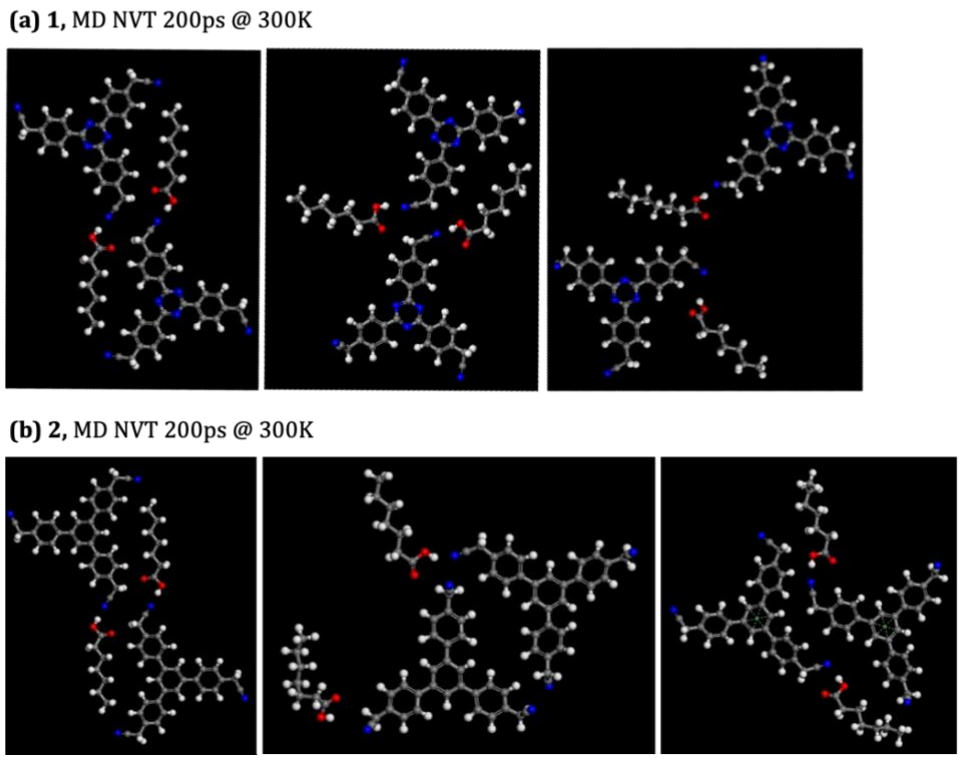

Figure S13. Snapshots of the MD simulations showing the potential contribution from the solvent in the stabilization of the networks for (a) **1** and (b) **2**.

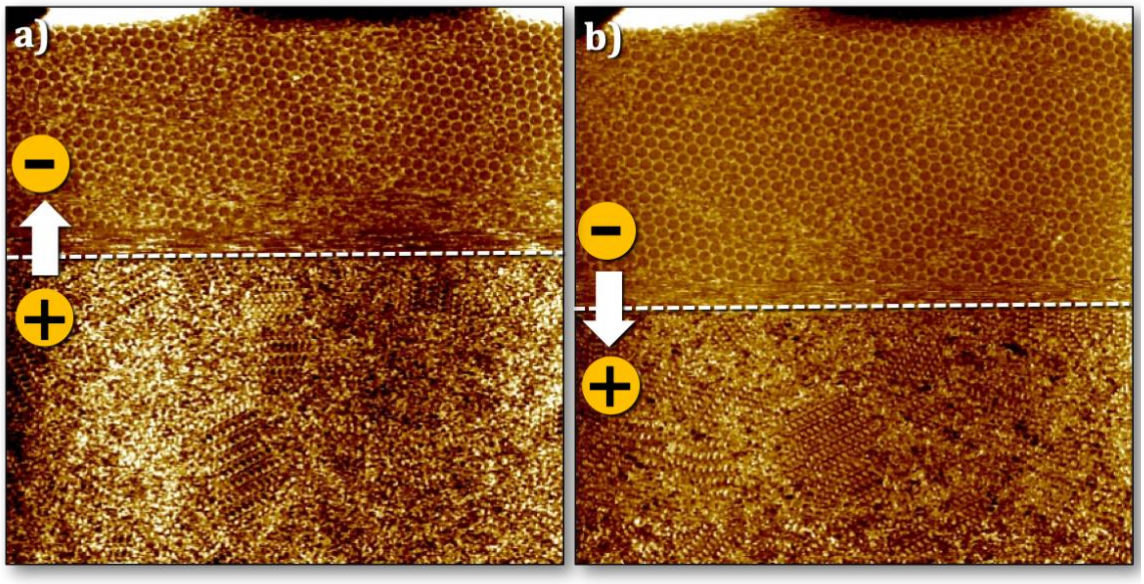

Figure S14. Additional STM data showing the bias-induced switching behavior of SAMNs of **1** at the OA/HOPG interface. Imaging parameters: (a) I_{set} = 100 pA, V_{bias} = +/−700 mV (b) I_{set} = 100 pA, V_{bias} = +/−700 mV (c) I_{set} = 100 pA, V_{bias} = +/−700 mV (d) I_{set} = 100 pA, V_{bias} = +/−700 mV.

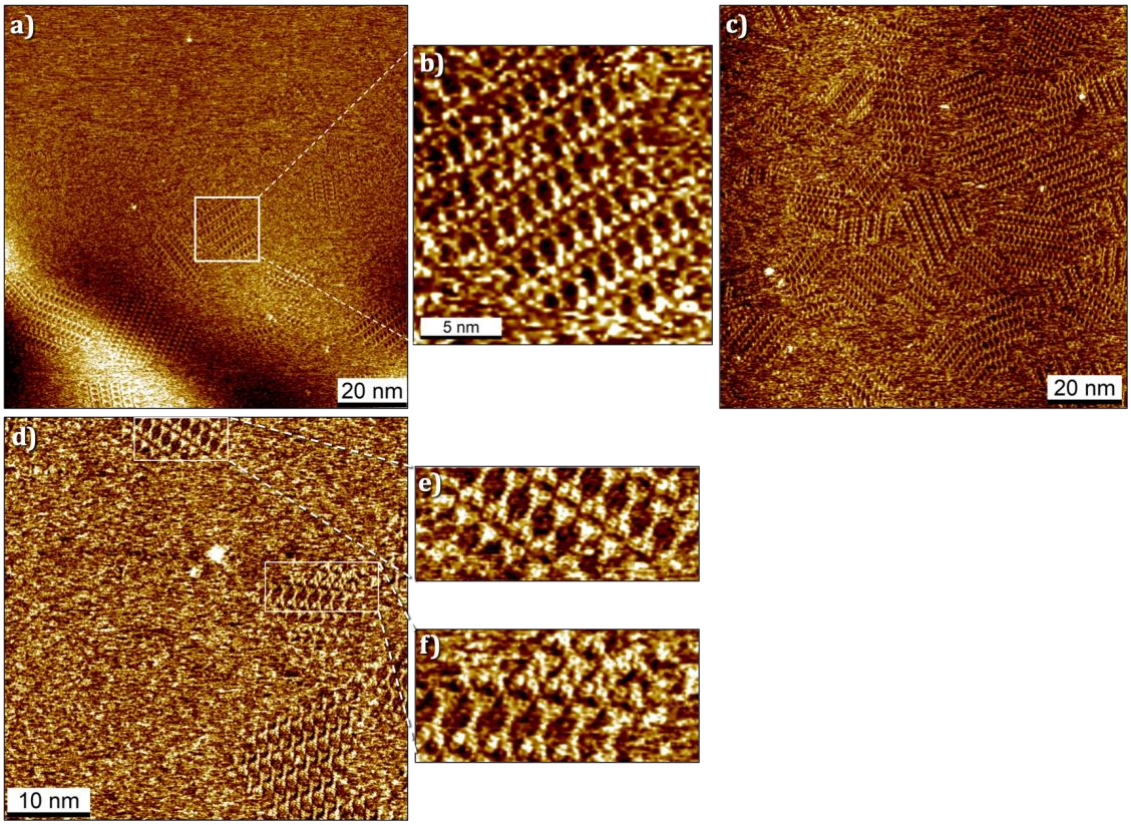

Figure S15. (a, c, d) Additional STM data showing the compact motifs formed by **1** under positive substrate bias at the OA/HOPG interface. (b, e, g) Digital zooms of the areas marked in the STM images provided in (a) and (d). Imaging parameters: (a) I_{set} = 100 pA, V_{bias} = +700 mV (c) I_{set} = 100 pA, V_{bias} = +700 mV. (d) I_{set} = 100 pA, V_{bias} = +700 mV

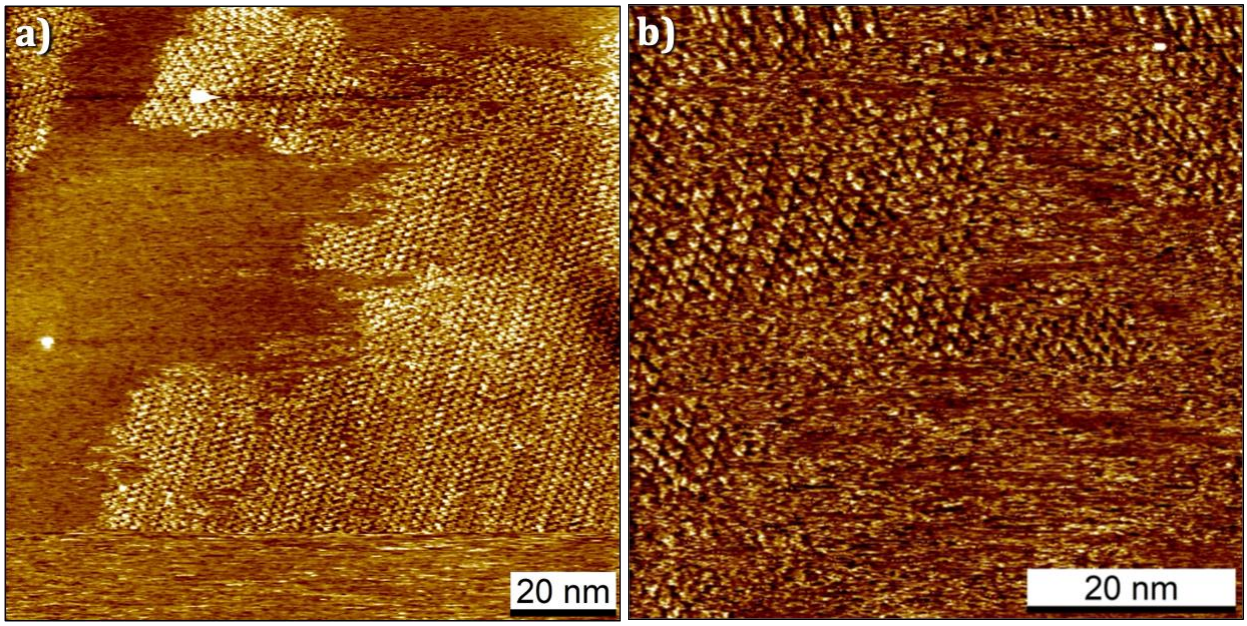

Figure S16. (a, b) Compact SAMN of **2** imaged at the OA/HOPG interface using STM. Imaging parameters: (a) I_{set} = 150 pA, V_{bias} = +300 mV (b) I_{set} = 150 pA, V_{bias} = +300 mV.

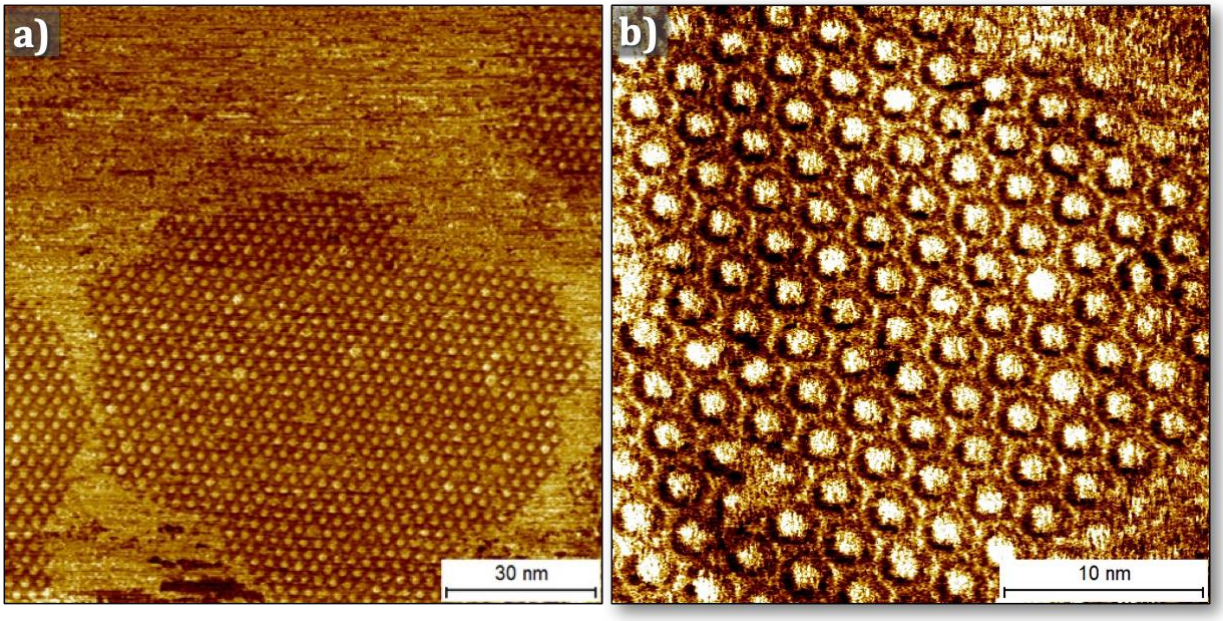

Figure S17. (a, b) Large and small scale STM images of the host-guest SAMN formed by 1 and coronene at the OA/graphite interface. Imaging parameters: (a) I_{set} = 100 pA, V_{bias} = -700 mV (b) I_{set} = 100 pA, V_{bias} = -700 mV.

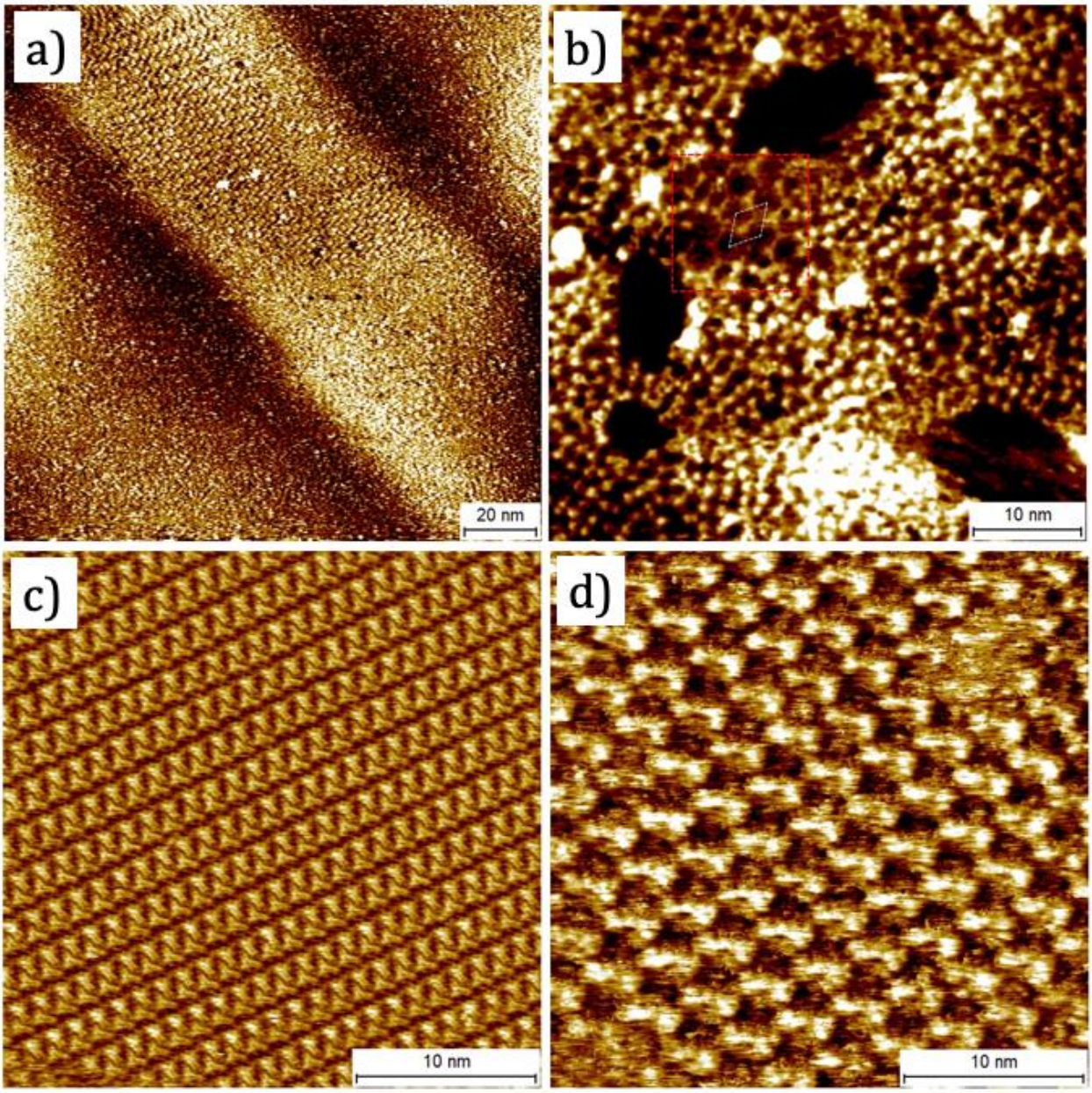

Figure S18. (a, b) STM images of the SAMN of molecule **1** at the HOPG/PO interface. In 1-PO, a predominantly amorphous network is observed, with only isolated hexagons (red square in b), highlighting the importance of solvent-mediated stabilization provided by octanoic acid. Imaging parameters: (a) I_{set} = 100 pA, V_{bias} = -700 mV, (b) I_{set} = 100 pA, V_{bias} = –1200 mV. (c, d) STM images of SAMN of **1** imaged at the OA/HOPG interface after (c) 2 days and (d) 4 days. When molecule **1** was deposited directly from the octanoic acid solution, no self-assembled network was observed immediately after or after a few hours from deposition. After two days, which was the standard window within which these SAMNs were characterized, we observed the formation of a dense network, which evolved into a porous network over four days. This indicates an extremely slow kinetics of formation for the porous network for compound **1**. Imaging parameters: (c) I_{set} = 100 pA, V_{bias} = -700 mV, (d) I_{set} = 120 pA, V_{bias} = –500 mV.

References:

(1) Fabozzi, F. G.; Severin, N.; Rabe, J. P.; Hecht, S. Room Temperature On-Surface Synthesis of a Vinylene-Linked Single Layer Covalent Organic Framework. *J. Amer. Chem. Soc.* **2023**, *145* (33), 18205-18209. DOI: 10.1021/jacs.3c04730.

(2) Becker, D.; Biswal, B. P.; Kaleńczuk, P.; Chandrasekhar, N.; Giebeler, L.; Addicoat, M.; Paasch, S.; Brunner, E.; Leo, K.; Dianat, A.; et al. Fully sp2-Carbon-Linked Crystalline Two-Dimensional Conjugated Polymers: Insight into 2D Poly(phenylenecyanovinylene) Formation and its Optoelectronic Properties. *Chem. Eur. J.* **2019**, *25* (26), 6562-6568. DOI: https://doi.org/10.1002/chem.201806385.

(3) Göller, A.; Grummt, U.-W. Torsional barriers in biphenyl, 2,2′-bipyridine and 2-phenylpyridine. *Chemical Physics Letters* **2000**, *321* (5), 399-405. DOI: https://doi.org/10.1016/S0009-2614(00)00352-3.